J|A|C|S ARTICLES

Published on Web 08/11/2010

Ordered Mesoporous Crystalline γ-Al_2O_3 with Variable Architecture and Porosity from a Single Hard Template

Zhangxiong Wu,[†,‡] Qiang Li,[‡] Dan Feng,[‡] Paul A. Webley,[†] and Dongyuan Zhao*[,†,‡]

Department of Chemical Engineering, Monash University, Clayton, Victoria 3800, Australia, and Department of Chemistry and Laboratory of Advanced Materials, Fudan University, Shanghai 200433, P. R. China

Received May 20, 2010; E-mail: dongyuan.zhao@eng.monash.edu.au; dyzhao@fudan.edu.cn

Abstract: In this paper, an efficient route is developed for controllable synthesis of ordered mesoporous alumina (OMA) materials with variable pore architectures and high mesoporosity, as well as crystalline framework. The route is based on the nanocasting pathway with bimodal mesoporous carbon as the hard template. In contrast to conventional reports, we first realize the possibility of creating two ordered mesopore architectures by using a single carbon hard template obtained from organic−organic self-assembly, which is also the first time such carbon materials are adopted to replicate ordered mesoporous materials. The mesopore architecture and surface property of the carbon template are rationally designed in order to obtain ordered alumina mesostructures. We found that the key factors rely on the unique bimodal mesopore architecture and surface functionalization of the carbon hard template. Namely, the bimodal mesopores (2.3 and 5.9 nm) and the surface functionalities make it possible to selectively load alumina into the small mesopores dominantly and/or with a layer of alumina coated on the inner surface of the large primary mesopores with different thicknesses until full loading is achieved. Thus, OMA materials with variable pore architectures (similar and reverse mesostructures relative to the carbon template) and controllable mesoporosity in a wide range are achieved. Meanwhile, *in situ* ammonia hydrolysis for conversion of the metal precursor to its hydroxide is helpful for easy crystallization (as low as ~500 °C). Well-crystallized alumina frameworks composed of γ-Al_2O_3 nanocrystals with sizes of 6−7 nm are obtained after burning out the carbon template at 600 °C, which is advantageous over soft-templated aluminas. The effects of synthesis factors are demonstrated and discussed relative to control experiments. Furthermore, our method is versatile enough to be used for general synthesis of other important but difficult-to-synthesize mesoporous metal oxides, such as magnesium oxide. We believe that the fundamentals in this research will provide new insights for rational synthesis of ordered mesoporous materials.

Introduction

Porous alumina materials offer a wide range of opportunities for industrial applications in adsorption, separation, catalysis, and/or catalyst support.[1−6] For a specific application under this wide spectrum, however, the pore structure and porosity of aluminas play a dominant role in their activity or/and affinity. Therefore, great efforts have been made to synthesize porous alumina materials with tailored structure and porosity.[7−13] Among them, fabrication of aluminas with ordered mesostructure and crystalline nature is of particular interest and in high demand, especially for shape-selective catalysis, molecular sieving, and selective adsorption of large molecules. However, there are limited reports on the synthesis of aluminas combining ordered mesostructure, large porosity, and highly crystalline nature with good thermal stability. Thus, it is still a large challenge but of great importance to prepare such alumina materials through an easy and flexible method.

State-of-the-art syntheses of ordered mesoporous materials include surfactant-directing and hard-templating routes.[14−16] However, both of these methods for the synthesis of ordered mesoporous

† Monash University.
‡ Fudan University.

(1) Karim, A. M.; Prasad, V.; Mpourmpakis, G.; Lonergan, W. W.; Frenkel, A. I.; Chen, J. G. G.; Vlachos, D. G. *J. Am. Chem. Soc.* **2009**, *131*, 12230.
(2) Sun, L. B.; Yang, J.; Kou, J. H.; Gu, F. N.; Chun, Y.; Wang, Y.; Zhu, J. H.; Zou, Z. G. *Angew. Chem., Int. Ed.* **2008**, *47*, 3418.
(3) Morris, S. M.; Fulvio, P. F.; Jaroniec, M. *J. Am. Chem. Soc.* **2008**, *130*, 15210.
(4) Kim, Y. H.; Kim, C. M.; Choi, I. H.; Rengaraj, S.; Yi, J. H. *Environ. Sci. Technol.* **2004**, *38*, 924.
(5) Trueba, M.; Trasatti, S. P. *Eur. J. Inorg. Chem.* **2005**, 3393.
(6) Marquez-Alvarez, C.; Zilkova, N.; Perez-Pariente, J.; Cejka, J. *Catal. Rev. Sci. Eng.* **2008**, *50*, 222.
(7) Yang, P. D.; Zhao, D. Y.; Margolese, D. I.; Chmelka, B. F.; Stucky, G. D. *Nature* **1998**, *396*, 152.
(8) Dacquin, J. P.; Dhainaut, J.; Duprez, D.; Royer, S.; Lee, A. F.; Wilson, K. *J. Am. Chem. Soc.* **2009**, *131*, 12896.
(9) Li, W. C.; Lu, A. H.; Schmidt, W.; Schüth, F. *Chem.—Eur. J.* **2005**, *11*, 1658.
(10) Matsui, Y.; Nishio, K.; Masuda, H. *Small* **2006**, *2*, 522.
(11) Deng, W. H.; Toepke, M. W.; Shanks, B. H. *Adv. Funct. Mater.* **2003**, *13*, 61.
(12) Zhang, W. Z.; Pinnavaia, T. J. *Chem. Commun.* **1998**, 1185.
(13) Boissiere, C.; Nicole, L.; Gervais, C.; Babonneau, F.; Antonietti, M.; Amenitsch, H.; Sanchez, C.; Grosso, D. *Chem. Mater.* **2006**, *18*, 5238.
(14) Kresge, C. T.; Leonowicz, M. E.; Roth, W. J.; Vartuli, J. C.; Beck, J. S. *Nature* **1992**, *359*, 710.
(15) Zhao, D. Y.; Feng, J. L.; Huo, Q. S.; Melosh, N.; Fredrickson, G. H.; Chmelka, B. F.; Stucky, G. D. *Science* **1998**, *279*, 548.
(16) Ryoo, R.; Joo, S. H.; Jun, S. *J. Phys. Chem. B* **1999**, *103*, 7743.

 10.1021/ja104379a

aluminas (OMAs) represent some considerable problems. For the former, susceptibility to hydrolysis of the aluminum precursors leads to wormhole-like or passably ordered mesopores with mainly amorphous walls in most cases.[7,11−13,17−23] Recently, Yuan et al. reported a reproducible route to the synthesis of thermally stable OMAs, but it requires a high temperature for crystallization of alumina (≥800 °C).[24] The latter nanocasting method, due to the diversity of hard templates and their rigid frameworks, which can effectively sustain local strains caused by crystallization, provides new opportunities for preparing many nonsiliceous ordered mesoporous materials with promising properties for designed applications.[25,26] However, the synthesis of OMAs also remains an experimental challenge because it is almost impossible to adopt the most available mesoporous silicas as hard templates due to the similarities in their chemistry. On the other hand, porous carbon materials are promising as hard templates for the synthesis of mesoporous crystalline metal oxides because they can provide the possibility of crystallization at high temperature under an inert atmosphere as well as easy removal by burn-out of the carbon template under air.[27−31] However, the synthesis procedure is somewhat laborious because pre-syntheses of both mesoporous silica and carbon hard templates are needed. More importantly, up to now, it has only been possible to get replicas with mesostructures that are the reverse of the hard templates in most nanocasting syntheses. There is a lack of flexible control of the mesopore architecture and porosity asssociated with using a single hard template.

Recently, a family of new ordered mesoporous carbon materials have been developed through an organic−organic self-assembly pathway.[32−34] Unlike the CMK-type carbon materials composed of nanowire arrays connected by small and short nanorods, FDU-type carbon materials have homologous carbon open frameworks with small micropores interpenetrating the thick mesopore walls. Moreover, they are easier and cheaper to apply for large-scale production, thus presenting new opportunities for synthesis of other important carbon-based mesoporous materials. However, in contrast to the CMK-type carbon materials, they have been not adopted as hard templates for the synthesis of other mesoporous materials, presumably because of their hydrophobic nature and the thick pore walls with only small micropores (mainly 0.7 and 1.1 nm) interconnecting the primary mesopores.[35] As a result, unlike the exo-templating of CMK-3 through coating the carbon nanowires from outside the mesopore surface, it is much more difficult for endo-templating to infiltrate metal precursors in the hydrophobic micropores of the FDU-type mesoporous carbon materials; it is extremely difficult to form stable connections penetrating the whole micropore walls. Therefore, rational design of pore size, pore interconnectivity, and surface chemistry for the FDU-type carbons is required in order to make them suitable as hard templates for the nanocasting synthesis of ordered mesoporous materials.

Herein, for the first time, by adopting an industry-scalable ordered mesoporous carbon from organic−organic self-assembly as a hard template, we report a facile route for not only synthesizing OMAs with crystalline pore walls but also readily controlling the mesopore architecture and porosity in a wide range. The success lies in the unique bimodal pore system with ordered primary mesopores interconnected by uniform complementary mesopores and surface functionalization of the carbon template. Through this method, we realize for the first time the possibility of fabricating ordered mesoporous metal oxides with variable pore architectures, especially pore networks both reverse and similar to the carbon hard template, by using a single template. The mesoporous alumina products possess readily controllable surface areas, pore volumes, and pore sizes, as well as crystalline mesopore walls with good thermal stability and high density of surface acidic and basic sites. Meanwhile, the synthesis is generally applicable for the fabrication of other mesoporous metal oxides such as MgO, paving the way for the synthesis of mesoporous materials through carbon nanocasting.

Experimental Section

Mesoporous Carbon Template. The pristine mesoporous carbon (PMC) template was prepared following a procedure similar to that reported by Liu et al.[36] Typically, 6.4 g of triblock copolymer Pluronic F127 ($(EO)_{106}(PO)_{70}(EO)_{106}$, Sigma-Aldrich Corp.) was dissolved in a mixture of 32.0 g of absolute ethanol and 4.0 g of 0.2 M HCl aqueous solution by stirring at 40 °C for 1 h. Then 8.32 g of tetraethoxysilane (TEOS, Sigma-Aldrich Corp.) and 20.0 g of 20 wt % ethanolic solution of resin precursor (resol) were added into the above solution and stirred for 2 h. The solution was cast on glass dishes, followed by evaporation of the solvents at room temperature for 5 h and heat treatment at 100 °C for 24 h. The polymer membranes were scraped off and ground into powders, followed by further polymerization and carbonization at 900 °C for 2 h with a ramp rate of 2 °C/min under nitrogen. Finally, the mesoporous carbon template was obtained by etching the silica component with a 10 wt % hydrofluoric acid solution (Sigma-Aldrich Corp.). (**Caution!** *HF is extremely hazardous. Special training and extreme care are needed when handling.*) The mesoporous carbon template thus-obtained was further surface-

(17) Fulvio, P. F.; Brosey, R. I.; Jaroniec, M. *ACS Appl. Mater. Interf.* **2010**, *2*, 588.
(18) Bai, P.; Wu, P.; Zhao, G.; Yan, Z.; Zhao, X. S. *J. Mater. Chem.* **2008**, *18*, 74.
(19) Cabrera, S.; El Haskouri, J.; Alamo, J.; Beltran, A.; Beltran, D.; Mendioroz, S.; Marcos, M. D.; Amoros, P. *Adv. Mater.* **1999**, *11*, 379.
(20) Zhang, Z. R.; Pinnavaia, T. J. *J. Am. Chem. Soc.* **2002**, *124*, 12294.
(21) Kuemmel, M.; Grosso, D.; Boissiere, U.; Smarsly, B.; Brezesinski, T.; Albouy, P. A.; Amenitsch, H.; Sanchez, C. *Angew. Chem., Int. Ed.* **2005**, *44*, 4589.
(22) Niesz, K.; Yang, P. D.; Somorjai, G. A. *Chem. Commun.* **2005**, 1986.
(23) Caragheorgheopol, A.; Rogozea, A.; Ganea, R.; Florent, M.; Goldfarb, D. *J. Phys. Chem. C* **2010**, *114*, 28.
(24) Yuan, Q.; Yin, A. X.; Luo, C.; Sun, L. D.; Zhang, Y. W.; Duan, W. T.; Liu, H. C.; Yan, C. H. *J. Am. Chem. Soc.* **2008**, *130*, 3465.
(25) (a) Schüth, F. *Angew. Chem., Int. Ed.* **2003**, *42*, 3604. (b) Ma, C. Y.; Mu, Z.; Li, J. J.; Jin, Y. G.; Cheng, J.; Lu, G. Q.; Hao, Z. P.; Qiao, S. Z. *J. Am. Chem. Soc.* **2010**, *132*, 2608.
(26) (a) Yang, H. F.; Zhao, D. Y. *J. Mater. Chem.* **2005**, *15*, 1217. (b) Wan, Y.; Yang, H. F.; Zhao, D. Y. *Acc. Chem. Res.* **2006**, *39*, 423. (c) Wan, Y.; Shi, Y. F.; Zhao, D. Y. *Chem. Commun.* **2007**, 897.
(27) Lu, A. H.; Schmidt, W.; Taguchi, A.; Spliethoff, B.; Tesche, B.; Schüth, F. *Angew. Chem., Int. Ed.* **2002**, *41*, 3489.
(28) Lai, X. Y.; Li, X. T.; Geng, W. C.; Tu, J. C.; Li, J. X.; Qiu, S. L. *Angew. Chem., Int. Ed.* **2007**, *46*, 738.
(29) Roggenbuck, J.; Tiemann, M. *J. Am. Chem. Soc.* **2005**, *127*, 1096.
(30) Liu, Q.; Wang, A. Q.; Wang, X. D.; Zhang, T. *Chem. Mater.* **2006**, *18*, 5153.
(31) Liu, Q.; Wang, A. Q.; Xu, J. M.; Zhang, Y. H.; Wang, X. D.; Zhang, T. *Microporous Mesoporous Mater.* **2008**, *116*, 461.
(32) Meng, Y.; Gu, D.; Zhang, F. Q.; Shi, Y. F.; Yang, H. F.; Li, Z.; Yu, C. Z.; Tu, B.; Zhao, D. Y. *Angew. Chem., Int. Ed.* **2005**, *44*, 7053.
(33) Zhang, F. Q.; Meng, Y.; Gu, D.; Yan, Y.; Yu, C. Z.; Tu, B.; Zhao, D. Y. *J. Am. Chem. Soc.* **2005**, *127*, 13508.
(34) (a) Meng, Y.; Gu, D.; Zhang, F. Q.; Shi, Y. F.; Cheng, L.; Feng, D.; Wu, Z. X.; Chen, Z. X.; Wan, Y.; Stein, A.; Zhao, D. Y. *Chem. Mater.* **2006**, *18*, 4447. (b) Wan, Y.; Shi, Y. F.; Zhao, D. Y. *Chem. Mater.* **2008**, *20*, 932.
(35) Wu, Z. X.; Yang, Y. X.; Tu, B.; Webley, P. A.; Zhao, D. Y. *Adsorption* **2009**, *15*, 123.
(36) Liu, R. L.; Shi, Y. F.; Wan, Y.; Meng, Y.; Zhang, F. Q.; Gu, D.; Chen, Z. X.; Tu, B.; Zhao, D. Y. *J. Am. Chem. Soc.* **2006**, *128*, 11652.

functionalized with nitric acid, yielding the functionalized mesoporous carbon (FMC) template with a high density of surface oxides.[37] The typical FMC template for the synthesis of mesoporous aluminas was obtained by treating the PMC template in a 5.0 M nitric acid solution at 40 °C for 3 h.

Mesoporous Alumina. Both the PMC and FMC templates were adopted as hard templates for the synthesis of mesoporous aluminas. In a typical procedure, 1.0 g of the FMC template was dispersed in 8.0 g of absolute ethanol. The calculated amount (2.67 g, 7.1 mmol) of $Al(NO_3)_3 \cdot 9H_2O$ (Merck Chemicals), based on the pore volume of the carbon template and the density of the alumina precursor, was then dissolved in ethanol (20 wt %) and added into the template dispersion, followed by stirring in a fume cupboard to evaporate the ethanol solvent and drying at 60 °C under vacuum for 3 h. The powder was then put into a small glass tube which was further put into a Teflon (polytetrafluoroethylene) bottle containing a ~14 wt % ammonia solution (~10 mL), without direct contact of the powder and the ammonia solution. After sealing, the bottle was heated in an oven at 60 °C for 3 h to hydrolyze the metal precursor in situ. After cooling to room temperature, the product was filtered and washed with small amount of water and ethanol to remove the possible soluble aluminum hydroxide located outside of the mesopores of the template and also the explosive NH_4NO_3 byproduct. After drying, the powder was calcined at 500 °C for 1 h to obtain the intermediate of alumina@carbon composites. The composites were then further impregnated with an appropriate amount of metal precursor and converted to alumina by the procedure described above. Two or three cycles of this procedure were needed in order to get ordered mesostructured products [~1.75 g (4.7 mmol) and ~1.32 g (3.5 mmol) of $Al(NO_3)_3 \cdot 9H_2O$ used for the second and third cycles, respectively]. Finally, the composites were calcined at 600 °C for 1 h under first N_2 and then air for 5 h to combust the carbon template. The mesoporous alumina products were denoted as OMA-*x*-FMC and MA-*x*-PMC for the functionalized and pristine mesoporous carbon templates, respectively, where *x* stands for the cycles of precursor impregnation and conversion processes.

Measurements and Characterization. X-ray diffraction (XRD) patterns were recorded with a Bruker D4 X-ray diffractometer (Germany) with Ni-filtered Cu Kα radiation (40 kV, 40 mA). Small-angle X-ray scattering (SAXS) patterns were recorded on a Nanostar U small-angle X-ray scattering system (Germany) using Cu Kα radiation (40 mV, 35 mA). Scanning electron microscopy (SEM) images were taken by a field-emission JEOL 6300F scanning electron microscope (Japan) or/and a Hitachi S4800 scanning electron microscope (Japan). Transmission electron microscopy (TEM) experiments were conducted on a Philips FEI CM200 microscope (Netherlands) or/and a JEOL 2100F microscope (Japan) operated at 200 kV. The samples for TEM measurements were suspended in ethanol and dropped onto holey carbon films supported on Cu grids. Nitrogen adsorption/desorption isotherms were measured at −196 °C with a Micromeritics ASAP 2020 analyzer. Before the measurements, the samples were degassed in a vacuum at 180 °C for at least 8 h. The Brunauer−Emmett−Teller (BET) method was utilized to calculate the specific surface area (S_{BET}) using adsorption data at $p/p_0 = 0.05-0.25$. The pore size distribution (PSD) was derived from the adsorption branch by using the Barrett−Joyner−Halenda (BJH) model. The total pore volume (V_t) was estimated from the adsorbed amount at $p/p_0 = 0.995$. Thermogravimetric analysis (TGA) was conducted on a Mettler Toledo TGA/SDTA851 analyzer (Switzerland) from 25 to 900 °C (5 °C/min) under oxygen (20 mL/min).

Results and Discussion

Ordered Mesoporous Aluminas with Different Pore Architectures. SEM images show that the FMC template has a flake-like morphology with ordered mesostructure (Supporting Information, Figure S1a,b). The mesoporous alumina materials OMA-2-FMC and OMA-3-FMC obtained by the nanocasting method for two and three impregnation−conversion cycles can retain the morphology (Figure S1c,d) as well as the ordered mesostructure of the carbon template, indicating a faithful replication. High-resolution SEM (HR-SEM) images show that both samples OMA-2-FMC (Figure 1a) and OMA-3-FMC (Figure 1b,c) possess ordered hexagonal mesostructure in a large domain, indicating an inherited mesostructure from the carbon template. Interestingly, large differences in the pore architectures between the two mesoporous alumina materials are clearly observed. First, the pore size of the sample OMA-2-FMC prepared from two impregnation−conversion cycles, roughly estimated from the HR-SEM images, is much larger than that of OMA-3-FMC from three cycles, and the pore network is more open, with more and larger complementary pores. This is even more obvious compared with the sample OMA-1-FMC obtained from only one cycle (Figure 1d), from which wide gaps can be observed between adjacent mesopore walls. This observation can be reasonably ascribed to the partial filling effect in the OMA-1-FMC and OMA-2-FMC cases. Second, due to the partial filling and the existence of many irregular complementary pores in the sample OMA-2-FMC, there are many defects on the pore surface. As a result, it is difficult to observe the ordered honeycomb structure along the [001] direction, while it can be observed in the sample OMA-3-FMC (Figure 1c). Nevertheless, tubular mesopores for the mesoporous alumina OMA-2-FMC are clearly observed along the [001] direction (Figure 1a inset, also see Figure S2), while no such tubular pores are observed in the sample OMA-3-FMC, indicating that the pore architectures for the two mesoporous alumina samples are obviously different, which will be discussed in detail later.

TEM (Figure 2a) shows that the ordered mesostructure can impenetrate one whole particle of the sample OMA-2-FMC with a size of about 1.4 μm (magnification of the image is needed to observe the ordered mesostructure), further indicating a faithful mesostructure replication. High-magnification TEM images of the mesoporous aluminas OMA-2-FMC (Figure 2b−d) and OMA-3-FMC (Figure 2e,f), together with the insets corresponding to fast Fourier transformation (FFT) patterns, further confirm that the mesopores are aligned in a 2-D hexagonal array, the same as in the FMC template. HR-TEM (Figure 2d) clearly shows the coexistence of mesostructural and atomic orderings (also see Figure S3), suggesting a crystalline pore wall. The selected area electron diffraction (SAED) pattern (Figure 2d, inset) shows distinctive diffraction rings which are well matched to the lattice *d*-spacing of γ-Al_2O_3, further confirming that the frameworks are composed of nanocrystals. The size of γ-Al_2O_3 nanocrystals is measured from the TEM observations to be about 6−7 nm. The energy-dispersive X-ray (EDX) spectrum (Figure 2g) shows that the framework is only composed of Al and O with a molar ratio close to the theoretic value of 2:3. In accordance with SEM observations, TEM measurements also show that the mesopore size of the sample OMA-2-FMC is larger than that of the OMA-3-FMC counterpart (comparing Figure 2b,c and e,f), and there are many small, complementary pores penetrating the pore walls and interconnecting with the primary mesochannels of the sample OMA-2-FMC, while far fewer such small pores are observed in the sample OMA-3-FMC (it can be observed by comparing the cylindrical pore walls in Figure 2b and e, also see Figure S4). The possible pore models for both samples are shown in Scheme 1, which will be discussed in more detail later.

(37) Wu, Z. X.; Webley, P. A.; Zhao, D. Y. *Langmuir* **2010**, *26*, 10277.

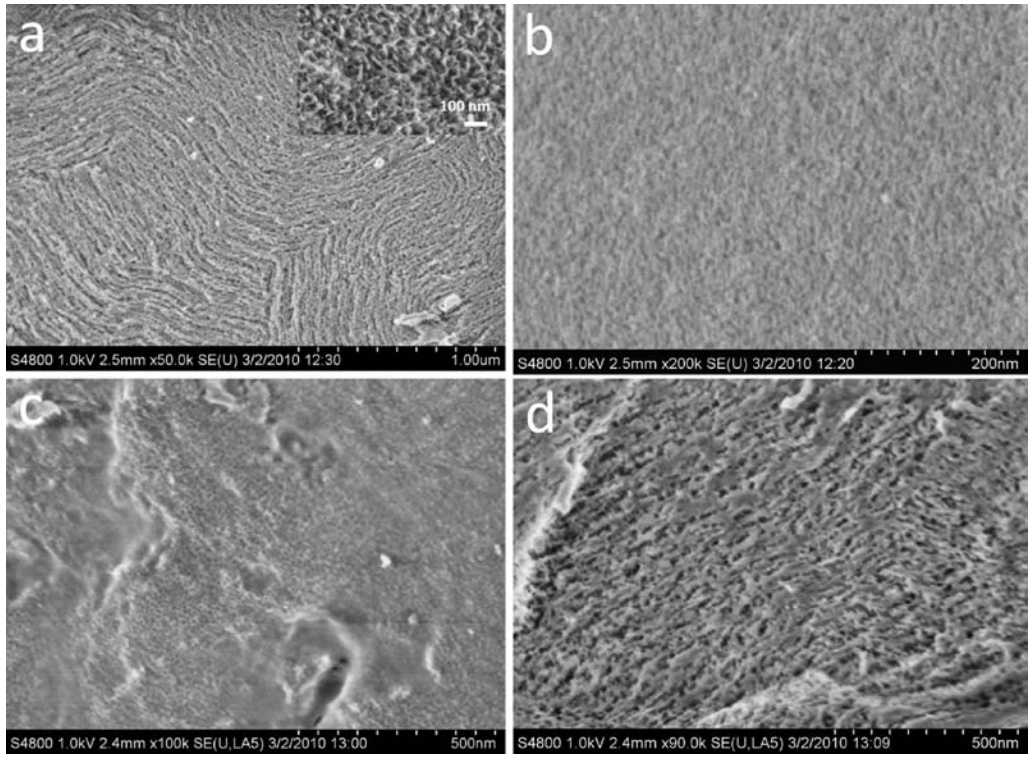

Figure 1. HR-SEM images of the mesoporous alumina materials: (a) OMA-2-FMC, (b,c) OMA-3-FMC, and (d) OMA-1-FMC. Inset (a) is a typical side view of the ordered mesopore domain presented in (a).

Wide-angle XRD patterns (Figure 3A) of the mesoporous alumina materials OMA-2-FMC and OMA-3-FMC both show well-resolved diffractions peaks which are well-matched to γ-Al_2O_3 (JCPDS 10-0425), suggesting that their frameworks are crystalline. The sizes of the γ-Al_2O_3 nanocrystals are evaluated to be about 7 nm on the basis of the Scherrer equation, in accordance with TEM observations. Such an easy crystallization at a low temperature (600 °C) is advantageous over the formation of soft-templated mesoporous alumina. SAXS patterns (inset Figure 3A) show low-intensity and wide scattering peaks, indicating the existence of only moderately ordered mesostructure which is much inferior to that of the template. It may be caused by partial collapse of the mesostructure during the processes of crystallization and burn-out of the carbon template. No scattering peak is observed in the SAXS pattern of the sample OMA-1-FMC (data not shown), in spite of the trend of hexagonal alignment of the pore walls in the SEM image (Figure 1d), suggesting that a suitable loading level is necessary to maintain the ordered mesostructure. Meanwhile, the sample OMA-3-FMC shows a more resolved SAXS pattern than that of OMA-2-FMC, suggesting that better regularity is achieved at higher precursor loading.

N_2 sorption isotherms (Figure 3B) of the two samples OMA-2-FMC and OMA-3-FMC both show typical type-IV curves, with a distinct condensation step and a hysteresis loop, revealing characteristics of mesoporous materials with narrow PSD (Figure 3B inset). The mesoporous alumina OMA-2-FMC shows a much larger pore size ($\sim$5.8 nm), higher surface area (261 m^2/g), and higher pore volume (0.45 cm^3/g) than those (3.6 nm, 158 m^2/g, and 0.17 cm^3/g) of the OMA-3-FMC counterpart (Table 1). Moreover, it also shows high liquid N_2 uptake at a low p/p_0 value (<0.1) with a PSD centered at $\sim$1.7 nm (Figure S5), indicating many small, complementary micropores, while the OMA-3-FMC counterpart shows far fewer such micropores, in accordance with SEM and TEM observations. Further direct evidence to demonstrate the different mesopore architectures in the two samples is based on the shapes of their hysteresis loops. Namely, the sample OMA-2-FMC possesses an H1-type hysteresis loop (Figure 3B, a), suggesting regularly cylindrical mesopores with a positive pore structure similar to that of the carbon template. In contrast, the sample OMA-3-FMC shows an H2-type hysteresis loop (Figure 3B, b), which originates from stacked mesopores of a mesostructure reverse to the carbon hard template. Therefore, it is concluded that OMAs with two different pore architectures are obtained (Scheme 1) by simply controlling the precursor loadings.

Formation Process of the Ordered Mesoporous Aluminas. With such a functionalized and bimodal mesoporous carbon as a hard template, we can finely tune the synthesis procedure and thus easily manipulate the pore architecture and porosity in a wide range. With a loading amount of about 40 wt % alumina in the composites (two cycles of impregnation−conversion), most of the small mesopores (2.3 nm) are fully filled, and the inner surfaces of the primary mesopores (5.9 nm) are probably coated with an alumina layer (Scheme 1a). Evidence is as follows: (1) compared to the carbon parent (Figure 4a), the N_2 sorption isotherms and the corresponding PSDs of the intermediate OMA-2@FMC (Figure 4b) composite show a much lower N_2 sorption amount, disappearance of the 2.3-nm small mesopore distribution, and a shift of the 5.9-nm primary mesopore distribution to 4.5 nm; (2) the TEM image (Figure S6) of the OMA-2@FMC intermediate shows smaller and lower-contrasted mesopores compared to the template (Figure S6a). We deduce that this pore-filling effect partially resembles that for mesoporous carbon CMK-5.[38] In our case, the complementary pores with abundant surface oxygen-containing groups are large in size (2.3 nm) and can easily accommodate the alumina precursors. As a result, stable alumina networks can

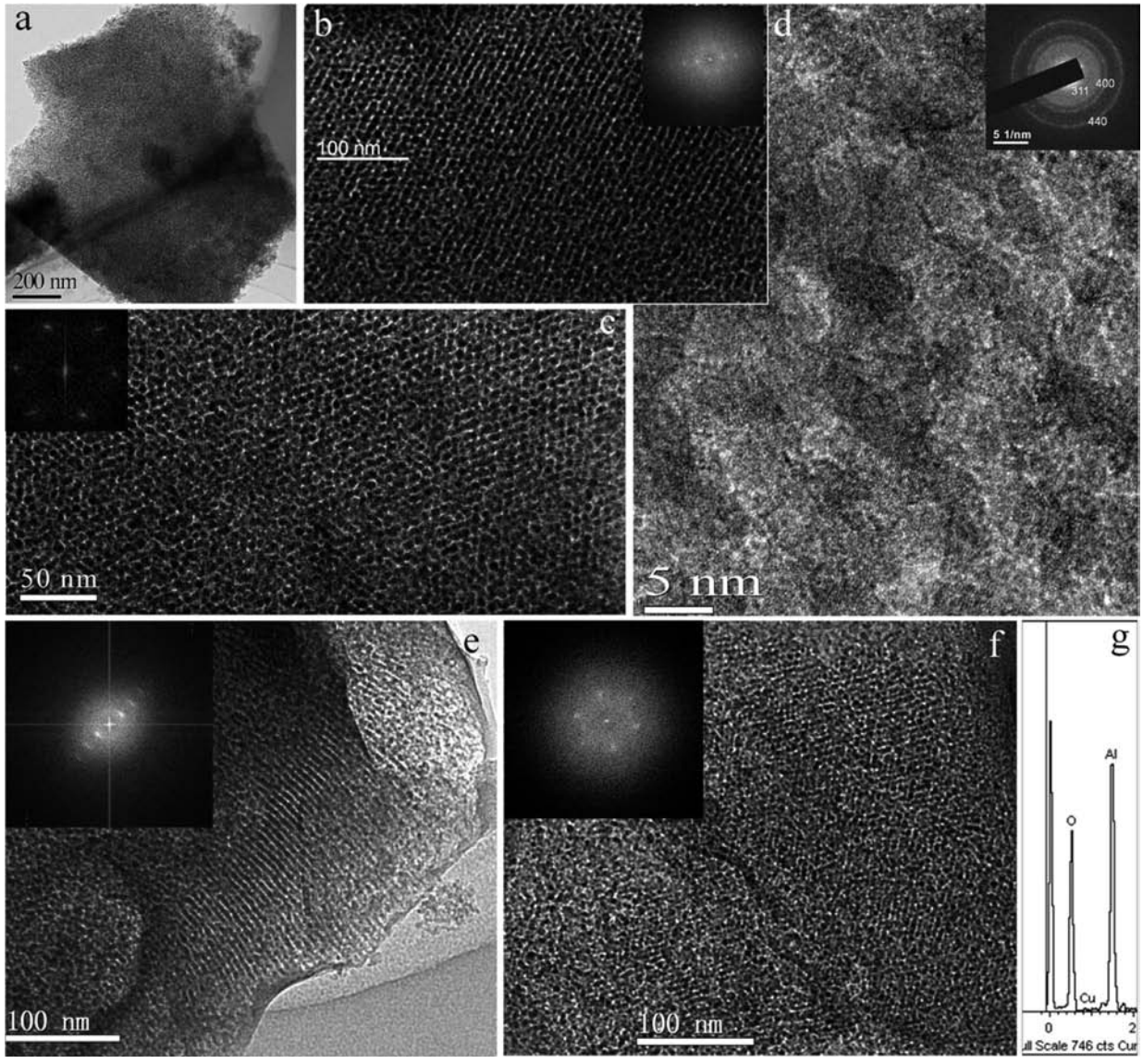

Figure 2. TEM images and inset corresponding FFT patterns of the mesoporous alumina OMA-2-FMC (a−c) and OMA-3-FMC (e,f) along typical directions. HR-TEM image and inset corresponding SAED pattern (d) and the corresponding EDX spectra (g) of the sample OMA-2-FMC.

Scheme 1. Schematic Representation of the Synthesis Process for the Ordered Mesoporous γ-Al_2O_3 Materials with Mesopore Architectures Both Similar to and Reverse of the Carbon Template[a]

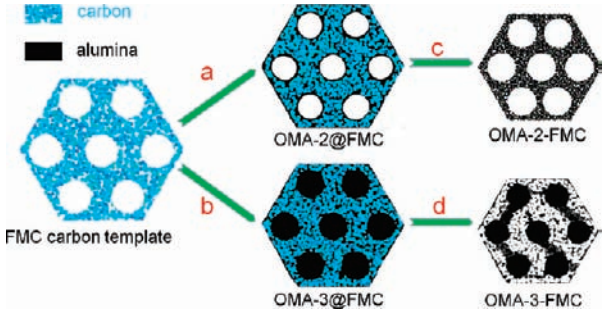

[a] The mesoporous alumina@carbon composites obtained by two (a) and three (b) cycles of impregnation−conversion; continuous (c) and replicated (d) alumina pore networks similar to and reverse of the mesoporous carbon template after crystallization and combustion of the carbon template, respectively.

be formed first in the small, complementary mesopore system (Scheme 1a). However, after removal of the carbon template, unlike CMK-5 carbon, the OMA-2-FMC product shows an H1-

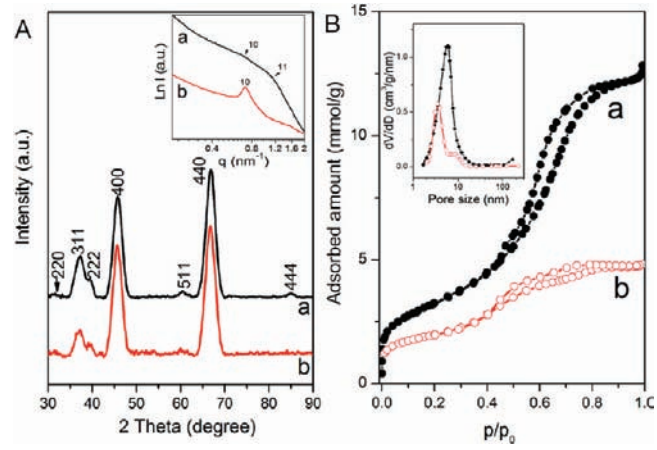

Figure 3. Wide-angle XRD and inset corresponding SAXS patterns (A) and N_2 sorption isotherms and inset pore size distribution curves (B) of the ordered mesoporous alumina materials OMA-2-FMC (a) and OMA-3-FMC (b). The arrows in the SAXS pattern of OMA-2-FMC are supposed to be the peak positions of the 10 and 11 scatterings.

Table 1. Structural and Textural Properties of the Pristine Mesoporous Carbon (PMC) and Functionalized Mesoporous Carbon (FMC) Templates and the Resultant Mesoporous Alumina Materials

material	a_0[a] (nm)	S_{BET}[b] (m^2/g)	V_{total}[c] (cm^3/g)	D[d] (nm)
PMC	11.0	1986	1.67	2.3, 5.9
FMC	11.2	1891	1.55	2.3, 5.9
OMA-1-FMC		332	0.84	8.0
OMA-2-FMC	9.7	261	0.45	5.8
OMA-3-FMC	9.6	158	0.17	3.6
MA-1-PMC		357	0.61	5.6
MA-2-PMC		265	0.36	4.2
MA-3-PMC		141	0.16	4.1

[a] Cell parameters were calculated from the SAXS patterns. [b] Surface areas were obtained by the BET method using adsorption data in p/p_0 range from 0.05 to 0.25. [c] Total pore volumes were estimated from the adsorbed amount at $p/p_0 = 0.995$. [d] Pore sizes were derived from the adsorption branches of the isotherms by using the BJH method.

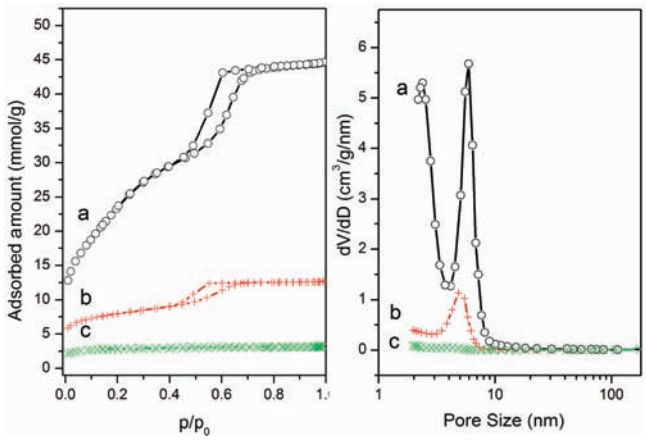

Figure 4. N_2 sorption isotherms (left) and the corresponding pore size distribution curves (right) of the functionalized mesoporous carbon template (a), the composites OMA-2@FMC (b), and OMA-3@FMC (c).

type hysteresis loop, a bimodal mesopore with a 5.8-nm primary mesochannel almost equal to the template, and a complementary pore centered at ~1.7 nm (Figure S5a,b). Moreover, tubular bimodal mesopores are also observed in SEM images (Figure 1a, inset and Figure S2), indicating a continuous pore system analogous to the template (Scheme 1c). The failure to obtain ordered nanopipes like CMK-5 is probably attributed to the different behaviors of metal oxide and carbon under thermal treatment. While the volume swells during the carbonization of the carbon precursor for CMK-5 case, the conversion and crystallization processes of alumina are accompanied by severe volume shrinkage. Meanwhile, the carbon template could be shaped at high temperature due to its surface oxides and the oxygen-rich alumina precursor. This sintering effect finally results in an obvious decrease of the unit cell (Table 1) and the loss of ordered nanopiped mesostructures, with only irregular tubular mesopores. For the sample OMA-2-FMC, the primary mesopore (5.8 nm) is inherited from the mesochannels of the carbon mother template, while the 1.7-nm pore probably originates from the carbon walls but loses its regularity because of the sintering effect. On the other hand, with a higher alumina loading up to ~52 wt % (three cycles), the mesopore network of the resultant mesoporous alumina OMA-3-FMC changes to another architecture, inverse to the template (Scheme 1b,d). The OMA-3@FMC composites show quite limited N_2 adsorption and disappearance of all peaks in the PSD curve (Figure 4c). Meanwhile, the TEM image shows that the mesopores and pore walls could not be differentiated (Figure S6c), indicating almost a full loading (Scheme 1b). This case is somewhat similar to the synthesis of mesoporous carbon CMK-3 replica, in which the carbon is fully filled in the whole channels of mesoporous silica SBA-15 template.[39] However, in our case, a large shrinkage of the carbon template occurred during the synthesis. The shrinkage shared the full loading effect, resulting in very low N_2 uptake (Figure 4c); otherwise, 52 wt % of alumina (three cycles) is not enough to fully fill the channels based on the pore volume of the mesoporous carbon template. Nevertheless, under such conditions, an ordered reverse mesostructure is obtained after removing the carbon template (Scheme 1d). The pore size (3.6 nm) of the sample OMA-3-FMC is due to the carbon wall of the template, but a little smaller as a result of crystallization. Meanwhile, in addition to the 3.6-nm mesopore, the sample OMA-3-FMC also shows a very weak PSD peak at ~6.8 nm (Figure 3B, b), probably due to a small fraction of partial filling effect in some domains. Moreover, overloading is also observed for the sample OMA-3-FMC. In some areas, thin and dense alumina layers coated on the ordered mesopore domains are observed (Figure S7), which may be a reason for the much lower surface area and pore volume compared with those of the sample OMA-2-FMC obtained from two cycles (Table 1).

Except for the above two cases of ordered mesopore architectures, we can also load alumina dominantly into the small mesopore and/or coat a layer of alumina with different thicknesses onto the inner surface of the primary mesopore of the carbon templates. As a result, mesoporous aluminas with variable pore sizes (3.6−8.0 nm), surface areas (158−380 m^2/g), and pore volumes (0.17−0.84 cm^3/g) can be obtained by decreasing the precursor loading. For example, less or disordered mesostructure is obtained for the sample OMA-1-FMC (Figures 1d and S8a). Moreover, in some cases with very low alumina loading, bimodal mesoporous alumina (4.5 and 9.8 nm) with high surface area (up to 400 m^2/g) can be obtained (Figure S9).

Effect of Synthesis Factors on Structure. In our synthesis, surface functionalization is crucial for faithful replication of the ordered mesostructure. Surface functionalization with HNO_3 can generate an abundance of carbon oxide species with no obvious influences on the mesostructure and texture of the template (Figures S10 and S11).[37] This functionalization changes the carbon template from mainly hydrophobic to hydrophilic because of the high density of oxygen-containing groups (especially hydroxyl and carboxyl). Thus, the alumina precursor can easily infiltrate deep into the small mesopores (2.3 nm), realizing the possible formation of stable alumina networks within the complementary pores on the carbon walls, which could then transfer to robust connections of the alumina to maintain the ordered mesostructure. Moreover, because of the strong interaction between the basic sites of alumina and acidic carbon oxides of the template, alumina coatings with different thicknesses are achievable. Evidence of such strong interactions is as follows: (1) the surface-functionalized mesoporous carbon template can trap a large amount of ammonia, even at high temperature,[37] and (2) CO_2 sorption results for the alumina materials exhibit a large amount of basic sites (about 535 μmol/

(38) Joo, S. H.; Choi, S. J.; Oh, I.; Kwak, J.; Liu, Z.; Terasaki, O.; Ryoo, R. *Nature* **2001**, *412*, 169.

(39) Jun, S.; Joo, S. H.; Ryoo, R.; Kruk, M.; Jaroniec, M.; Liu, Z.; Ohsuna, T.; Terasaki, O. *J. Am. Chem. Soc.* **2000**, *122*, 10712.

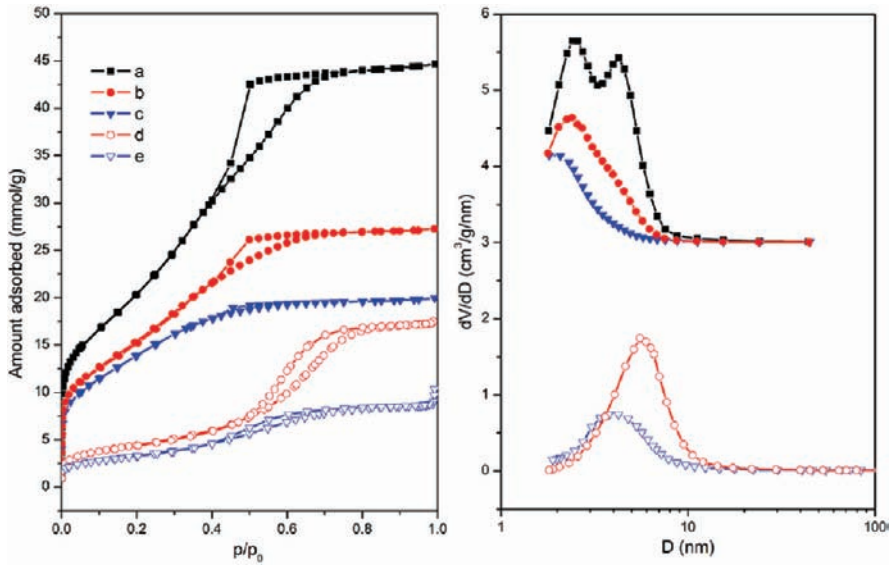

Figure 5. N_2 sorption isotherms (left) and the corresponding pore size distribution curves (right) of the pristine mesoporous carbon template (a), the mesoporous alumina@carbon composites MA-1@PMC (b) and MA-2@PMC (c), and mesoporous alumina MA-1-PMC (d) and MA-2-PMC (e), respectively.

g, see below). In contrast, our results show that, when the PMC without functionalization was adopted as the hard template, it was almost impossible to get any ordered mesostructure. In this case, the small, complementary mesopores and even some of the large primary mesopores are not accessible for the alumina precursor loading because of their hydrophobic nature, resulting in only partial filling and disordered aluminas. N_2 sorption isotherms of the MA@PMC composites templated by the PMC without functionalization under similar synthesis condition (Figure 5) present significant differences compared with those of the OMA@FMC counterparts (Figure 4). After two or three cycles of alumina precursor loading, the composites MA@PMC still show much larger BET surface area and pore volume than those of OMA@FMC counterparts with similar alumina contents. This indicates that a large fraction of mesopores of the pristine carbon template is inaccessible. In contrast to those for the OMA@FMC counterparts, N_2 sorption isotherms of all the MA@PMC composites show an almost unchanging behavior for the small, complementary mesopore (Figure 5b,c), clearly indicating that the small mesopores are inaccessible for alumina loading. These differences suggest that, for the functionalized carbon template, the alumina precursors infiltrate into the small mesopores as a priority, while only the primary mesopores are accessible for loading in the pristine carbon. N_2 sorption isotherms of the mesoporous alumina MA-*x*-PMC templated by the PMC also show typical type-IV curves with narrow PSDs (Figure 5d,e), with controllable surface areas of 141−381 m^2/g, large pore volumes of 0.16−0.67 cm^3/g, and uniform pore sizes at 4−9 nm (Table 1). As an example, SEM and TEM images show that the mesoporous MA-2-PMC material possesses the same flake-like morphology as the template (Figure 6a), uniform worm-hole-like mesopores (Figure 6b−d), and crystalline mesopore walls (Figure 6d, inset).

Our results show that the size of complementary mesopores (2.3 nm) also plays an important role for the replication of ordered mesostructure. When we chose the FMC FDU-15 with only complementary micropores (mainly 0.7 and 1.1 nm) as a hard template, it was almost impossible to obtain ordered mesostructured alumina (data not shown). This is because it is fairly difficult to infiltrate metal precursor into the micropores and form continuous connections on the pore walls of FDU-15. This effect of complementary pores was also reported when mesoporous silica was adopted as a hard template.[40]

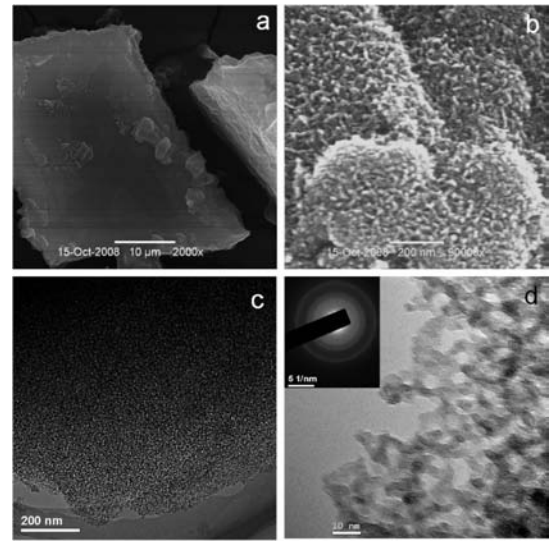

Figure 6. SEM images (a,b), TEM images (c,d), and the corresponding SAED pattern (inset d) of the mesoporous alumina MA-2-PMC sample.

Another unique feature of our synthesis is the conversion method. We found that *in situ* ammonia hydrolysis for converting the alumina precursor to its hydroxide is very helpful for easy crystallization at low temperatures. The mesoporous aluminas OMA-2-FMC and OMA-3-FMC obtained at 600 °C have good crystalline nature. We found that heating at about 500 °C can yield a mesoporous crystalline alumina. However, it is difficult to completely remove the carbon template under air below 600 °C. Without the *in situ* hydrolysis step, OMAs can also be obtained under the same condition as those for OMA-3-FMC (Figure S12a). However, the wide-angle XRD pattern shows that the product is mainly amorphous at 600 °C (Figure S13a). It needs a higher temperature (∼800 °C) to crystallize the framework (Figure S13b−d). Because of the high

(40) Wu, Z. X.; Meng, Y.; Zhao, D. Y. *Microporous Mesoporous Mater.* **2010**, *128*, 165.

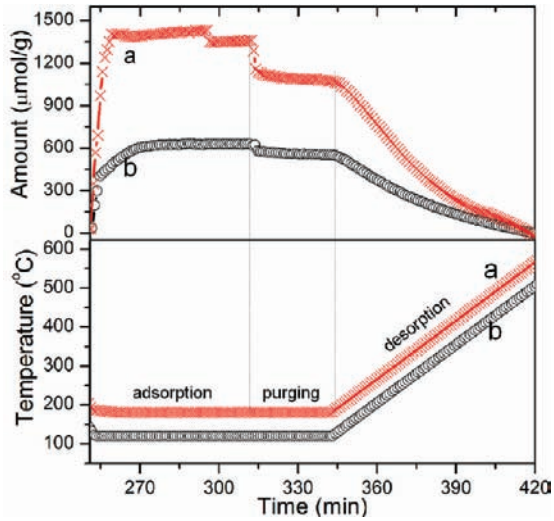

Figure 7. Ammonia (a) and carbon dioxide (b) adsorption and desorption properties on the ordered mesoporous alumina OMA-2-FMC. The sample was activated at 500 °C for 2 h before adsorption. Adsorption temperature of ammonia and carbon dioxide was set at 180 and 120 °C, respectively.

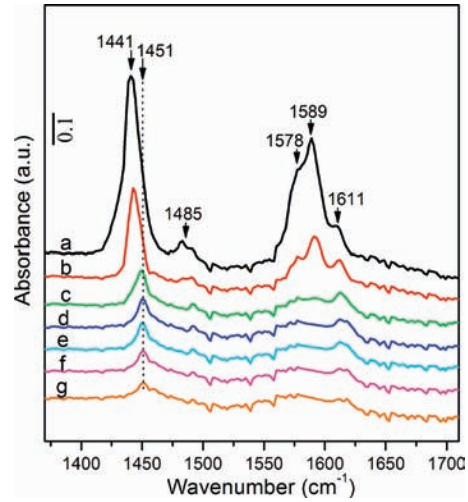

Figure 8. FTIR spectra of pyridine adsorption for the mesoporous OMA-2-FMC measured at (a) 25 °C after adsorption of pyridine and after desorption at (b) 25, (c) 100, (d) 150, (e) 200, (f) 250, and (g) 300 °C for 0.5 h.

temperature, the ordered mesostructure deteriorates substantially (Figure S12b−d). Moreover, *in situ* ammonia hydrolysis conversion is helpful for coating metal oxide on the pore surface of the carbon template and preventing aggregation of alumina particles,[41] which is otherwise clearly observed (Figure S14).

To further demonstrate the easy loading of alumina precursors after surface functionalization, we also adopted aqueous $AlCl_3$ solution as the precursor. Our results show that OMAs are again obtainable (Figure S8b), indicating that the carbon oxide species on the surface could guarantee infiltration of the alumina precursor deep into the complementary mesopores, even with water as a solvent. Meanwhile, our method is general and can be expanded for syntheses of other mesoporous metal oxides. For example, ordered mesoporous MgO products with defined mesoporosity and crystalline nature can be prepared (Figures S15 and S16), which are difficult to obtain from other methods (both soft and hard templating).

Thermal Stability and Surface Property. The thermal stability of the mesoporous alumina products was initially investigated. Heat treatment of the mesoporous alumina OMA-3-FMC sample under air at 700−900 °C for 1 h leads to deterioration or collapse of the ordered mesostructure, but the products still show similar morphology and high mesoporosity (Figures S17 and S18), suggesting a good thermal stability of the framework.

The mesoporous alumina OMA-2-FMC shows high density of both acidity and basicity (Figure 7) (experimental details in Supporting Information). The density of acidity is estimated to be 1090 μmol of NH_3 per gram of alumina by integration of the profile of NH_3 adsorption at 180 °C and desorption up to 600 °C (Figure 7a). On the basis of an average value of 0.14 nm^2/molecule of the cross-section area of ammonia,[42] the active surface area (ASA) is calculated to be 91.8 m^2/g. This density of acidity and ASA seem much larger than the values for the mesoporous alumina reported previously,[17] probably attributed to the high crystallinity and unique mesopore architecture of our mesoporous alumina materials. Meanwhile, the density of basic sites is estimated to be 535 μmol/g, retrieved from the CO_2 adsorption at 120 °C and desorption up to 600 °C (Figure 7b), which is a little lower than the reported value.[17] The ASA calculated from CO_2 adsorption (0.218 nm^2/molecule) is 70.2 m^2/g, in accordance with the value retrieved from NH_3 adsorption. The high density of both acidic and basic sites, together with the special mesostructures and high porosities, suggests that these new mesoporous alumina materials could find great potential in catalysis as supports or catalysts.

The FTIR spectra of adsorbed pyridine on the mesoporous OMA-2-FMC display several characteristic bands (Figure 8).[43−45] The bands at ∼1441, 1485, and 1589 cm^{-1} are ascribed to the hydrogen-bonding between pyridine and the surface OH groups of alumina (aprotic sites). The bands at 1447−1451 and ∼1611 cm^{-1} are ascribed to the interaction between nitrogen lone-pair electrons and coordinatively unsaturated Al^{3+} ions (Lewis acid sites). On the other hand, the band at ∼1578 cm^{-1} is contributed by both of the above two sites. After evacuation at room temperature, the intensities of all the bands decrease (Figure 8b), indicating desorption of weakly adsorbed pyridine. Upon evacuation at higher temperatures (100−300 °C), the intensities of the bands at ∼1441, 1485, and 1589 cm^{-1} decrease dramatically (Figure 8c−g); it even almost disappears for the 1485 cm^{-1} band at 300 °C (Figure 8g). This behavior is due to the relatively weak interaction between pyridine and aprotic OH groups. Nevertheless, since the interactions between Lewis sites and pyridine are strong, the bands at ∼1451, 1578, and ∼1611 cm^{-1} can be clearly detected, even at 300 °C. Meanwhile, these bands shift to higher frequencies with increasing temperature because the coordination bond energy increases as well. Finally, the bands at 1639 and 1545 cm^{-1} assigned to Brönsted acid sites are not observed, indicating that there is basically no such acid type in the material.

Conclusion

We report a facile and controllable route for the synthesis of ordered mesoporous crystalline alumina materials with variable

(41) Krishnan, C. K.; Hayashi, T.; Ogura, M. *Adv. Mater.* **2008**, *20*, 2131.
(42) McClella, A. L.; Harnsber, H. F. *J. Colloid Interface Sci.* **1967**, *23*, 577.
(43) Abbattista, F.; Delmastro, S.; Gozzelino, G.; Mazza, D.; Vallino, M.; Busca, G.; Lorenzelli, V.; Ramis, G. *J. Catal.* **1989**, *117*, 42.
(44) Layman, K. A.; Ivey, M. M.; Hemminger, J. C. *J. Phys. Chem. B* **2003**, *107*, 8538.
(45) Ertl, G.; Knözinger, H.; Weitkamp, J. *Handbook of Heterogeneous Catalysts*; Wiley-VCH: New York, 1997; Vol. 2, p 710.

architecture and porosity from a single hard template. This is the first report that ordered mesoporous carbon from organic−organic self-assembly can be adopted as a hard template for the replication of ordered mesostructures. Moreover, it is also the first time that ordered metal oxides with different mesopore architectures (for example, pore networks reverse of and similar to the hard template) can be prepared by using a single hard template. We demonstrate that the unique bimodal mesopores and the surface oxides after functionalization of the carbon template, along with the *in situ* ammonia hydrolysis conversion method, guarantee the successful fabrication of ordered alumina mesostructure with crystalline framework, ready manipulation of pore architecture and texture properties, and easy crystallization (500 °C). Namely, the bimodal mesopores (2.3 and 5.9 nm) and the surface functionalities of the carbon template enable the selective loading of alumina precursors into the small mesopores dominantly or/and with a layer of alumina coated on the inner surface of the large primary mesopore channels with different thickness until a full loading, which provides a general protocol for controllable synthesis. The mesostructure and porosity of the mesoporous alumina products can be conveniently manipulated within a wide range, which can achieve high surface area (up to 400 m^2/g), large pore volume (up to ∼1.0 cm^3/g), and uniform pore size (from ∼3.6 to 9.0 nm). Well-crystallized alumina frameworks are composed of γ-Al_2O_3 nanocrystals of 6−7 nm size. Meanwhile, the mesoporous alumina materials have high-density sites of both acidity and basicity, which could be very useful in catalysis. Furthermore, such a novel strategy would pave the way for the synthesis of other metal oxides, such as MgO and ZnO, with controllable mesostructures and textures. We believe our synthesis would provide new insights for rational design and synthesis of ordered mesoporous materials.

Acknowledgment. We greatly appreciate financial support from the National Science Foundation and the State Key Basic Research Program of China and the Discovery grants from the Australian Research Council (DP0773160 and 0879769). Z.W. thanks the China Scholarship Council for financial support.

Supporting Information Available: Experimental details of ammonia and carbon dioxide adsorption and FTIR of pyridine adsorption; comprehensive supporting data of XRD patterns, N_2 sorption results, and microscope images of the carbon templates, composites, and alumina products; and results on ordered mesoporous MgO material. This material is available free of charge via the Internet at http://pubs.acs.org.

JA104379A